Available online at www.sciencedirect.com
SCIENCE DIRECT®
International Journal of Heat and Mass Transfer 47 (2004) 2689–2698
International Journal of HEAT and MASS TRANSFER
www.elsevier.com/locate/ijhmt

Bubble cavitation in a microchannel

J. Li [a], P. Cheng [b,*]

[a] Department of Mechanical Engineering, Hong Kong University of Science and Technology, Clear Water Bay, Kowloon, Hong Kong
[b] School of Mechanical and Power Engineering, Shanghai Jiaotong University, Shanghai 200030, PR China

Received 23 December 2002; received in revised form 15 November 2003

Abstract

The effects of microchannel size, mass flow rate and heat flux on boiling incipience or bubble cavitation in a microchannel are studied in this paper. The well-known concept of survival of a bubble cavity is extended, and the classical kinetics of nucleation is introduced to study bubble nucleation in water flowing in a silicon microchannel. The effects of contact angle, dissolved gas, and the existence of microcavities and corners in the microchannel on bubble's nucleation/cavitation temperature are estimated. With this information, a numerical solution is carried out to study the effects of mass flow rate and heat flux on bubble nucleation/cavitation in microchannels. The results of this analysis provide further physical insight on boiling heat transfer in microchannels.

Keywords: Bubble cavitation; Microchannel; Kinetics; Homogeneous nucleation; Heterogeneous nucleation

1. Introduction

Bubble nucleation in microchannels has attracted a great deal of interest in recent years. One of the reasons for this interest is because of its application to microelectronics cooling due to the miniaturization of the electronics devices that lead to denser packaging of components with associated higher heat fluxes [1]. Another reason for recent interest is because of its applications to vapor bubble actuation with pulsed heating in MEMS [2], e.g., ink jet printers [3], micropumps [4], micro-bubble motors and micro-bubble valves [5], etc.

The onset of bubble nucleation usually requires that the device temperature exceeds the saturation temperature of the liquid corresponding to a given pressure. In general, the liquid adjacent to the heated surface has to be superheated for the first bubble to be formed. The formation of vapor film [1] or vapor bubble [6] may partially block the microchannel leading to the overheating of the IC apparatus. Thus, in the implementation of phase-change schemes using dielectric coolant for cooling of microelectronic chips, the uncertainty of the initiating nucleate boiling that leads to potential damage of the device by thermal shocks must be taken into consideration. Based on Kwak's theory [7], Zhang et al. [6] discussed vapor bubbles damped by the pressure wave traveling in the liquid to explain the absence of vapor bubbles in a microchannel. Jiang et al. [8] made a visualization study on flow boiling in microchannels. Qu and Mudawar [9] performed both experimental and numerical studies on the effect of flow velocity on the incipient boiling heat flux in a microchannel. Most recently, Wu and Cheng [10,11] observed for the first time that three unstable boiling modes exist in parallel microchannels depending on the amount of heat flux.

There has been a great deal of analyses on bubble nucleation in pool boiling in macrosystems during the past few decades [12–15]. In particular, Hsu [12,13] has proposed a criterion for bubble survival in pool boiling in a heated cavity. Cole [14] as well as Blander and Katz [16] have performed analyses on homogeneous and heterogeneous nucleation on a surface with no cavities and with microcavities. While some of these analyses can be applied to microsystems with new interpretation [3], others are not directly applicable and need modifications. In this connection, it is important to recognize

* Corresponding author. Tel./fax: +86-21-6293-3107.
E-mail address: pingcheng@sjtu.edu.cn (P. Cheng).

0017-9310/$ - see front matter © 2003 Elsevier Ltd. All rights reserved.
doi:10.1016/j.ijheatmasstransfer.2003.11.020

Nomenclature

C_g	solubility of dissolved gas
C_P	specific heat
h	Prancle constant
h_{fg}	heat of evaporation
J	bubble nuclei density
k	Boltzmann constant
K_h	Henry's constant
L	length
N_0	molecule number per unit volume
P	pressure
P_{vb}	partial pressure of vapor phase
P_{gb}	partial pressure of gas phase
q_w	heat flux
r_c	critical bubble size
r_m	equivalent radius of a cavity
T	temperature
T_{nl}	nucleation temperature in liquid
T_l	liquid temperature of bulk
T_w	temperature at wall of microchannel
y_b	projection height of bubble over wall surface

Greek symbols

θ	contact angle (°)
β	half angle of corner of a microchannel or cavity (°)
γ	constant in Eq. (9)
σ	surface tension
λ	conductivity
ρ	density
μ	dynamic viscosity
υ	kinetic viscosity

Subscripts

b	bubble
het	heterogeneous nucleation
hom	homogeneous nucleation
in	parameters at inlet of microchannel
out	parameters at outlet of microchannel
s	saturated state
v	vapor
l	liquid
w	wall or substrate

that the characteristics of bubble cavitation in microchannels are somewhat different from those of the macrosystems owing to the following reasons:

(i) The surfaces manufactured by microfabrication technology are usually very smooth with sub-microcavities. For example, Lin [2] scanned the surface of a polysilicon microheater with an atomic force microscope (AFM) and found the mean square roughness to be 6.5 nm, which is of the same size of a critical vapor bubble. Thus, the dominant mechanism for bubble nucleation in microchannels is homogeneous nucleation or heterogeneous nucleation on a surface with nano/microsize cavities.
(ii) Since cross-sections of silicon microchannels are usually of trapezoidal, triangular, and rectangular shapes, the existence of corners in these microchannels may play an important role on the bubble nucleation process.
(iii) The liquid flow motion is likely to be laminar due to the small size of the microchannel and at low Re numbers.

The major objective of this paper is to study effects of microchannel size, mass flow rate, and heat flux on boiling incipience or bubble cavitation in liquid. To this end, the vapor temperature for homogeneous nucleation and heterogeneous nucleation on smooth surfaces applicable to microchannels will first be determined. The possible effects for lowering this nucleation temperature are discussed. In particular, we modify the classical theory of heterogeneous nucleation on smooth surfaces to estimate the effect of corners on nucleation temperature in microchannels. A numerical solution based on laminar convection heat transfer is obtained to study the incipient boiling in a microchannel by adopting Hsu's concept of bubble survival [12]. The effects of flow rate and heat flux on incipient boiling in a microchannel are discussed. The results of this analysis provide further physical insight on incipient boiling heat transfer in microchannels.

2. Hsu's criteria

We now briefly review Hsu's theory [12,13] for the survival of a vapor bubble in pool boiling in a cavity on a heated surface as shown in Fig. 1. Hsu [12] proposed that the vapor bubble in the cavity will begin to grow if

$$T_l(y_b) \geqslant T_b \tag{1}$$

where $T_l(y)$ is the temperature distribution in liquid near the heating surface which is given by

$$\frac{T_l(y) - T_\infty}{T_w - T_\infty} = \frac{\delta_T - y}{\delta_T} \tag{2}$$

where δ_T is the thickness of thermal boundary. Eq. (2) was obtained by solving the one-dimensional heat con-

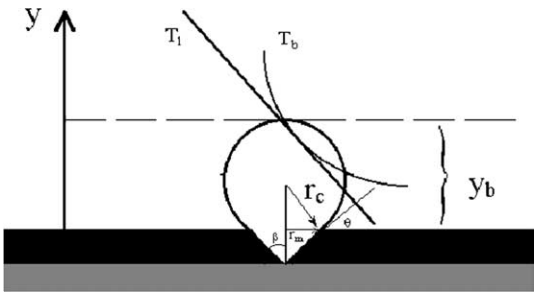

Fig. 1. Hsu's model for bubble survival in a cavity [12,13].

duction equation with constant wall temperature boundary condition. T_b in Eq. (1) is the vapor temperature in the bubble which can be determined from the Young–Laplace equation and the Clausius–Claperon equation

$$\frac{dT}{d\rho} = \frac{T}{h_{fg}\rho_v} \tag{3}$$

to give

$$T_b - T_s = \frac{c_1 2\sigma T_s}{c_2 h_{fg}\rho_v y_b} \tag{4a}$$

with

$$c_1 = 1 + \cos\theta, \quad c_2 = \frac{1}{\sin\theta}, \quad y_b = c_1 r_c, \quad r_c = c_2 r_m, \tag{4b}$$

where θ is the contact angle for solid–liquid interface, y_b is the projection height of vapor bubble over the surface and r_m is the given surface equivalent radius of the cavity (see Fig. 1). Based on thermodynamics consideration, Ward et al. [17] have proved that the necessary (but not sufficient) condition for the emergency of the trapped vapor bubble is $r_c = r_m$, for contact angle $\beta \leqslant \theta \leqslant \pi/2$, which is the thermodynamic mechanism of Hsu's criteria. Although Hsu's theory given by Eqs. 2,4a,4b is for pool boiling in a large cavity and is not applicable to bubble nucleation in liquid on a smooth surface such as those in silicon microchannels, his concept on bubble survival given by Eq. (1) will be extended and applied to identify incipient flow boiling in a microchannel as will be discussed in Section 4.

3. Bubble nucleation and cavitation temperatures in a microchannel

As mentioned earlier, vapor bubbles in microchannels may be generated in liquid (homogeneous nucleation), on a surface or at a corner (heterogeneous nucleation). In this section, we will discuss the bubble nucleation temperature and its initial size based on the classical kinetics of nucleation.

Thermodynamic and mechanical equilibrium on a curved vapor–liquid interface requires a certain degree of superheat in order to maintain a given curvature. The incipience temperature can be computed from the classical kinetics of nucleation [13–15]:

For homogeneous nucleation in superheated liquids

$$J_{hom} = N_0 \left(\frac{kT_{nl}}{h}\right) \exp\left[-\frac{16\pi\sigma^3}{3kT_{nl}(P_b - P_l)^2}\right] \tag{5}$$

For heterogeneous nucleation on surface

$$J_{het} = N_0^{2/3}\psi \left(\frac{kT_{nl}}{h}\right) \exp\left\{-\frac{16\pi\sigma^3\omega}{3kT_{nl}(P_b - P_l)^2}\right\} \tag{6}$$

where J is the bubble nucleation density. In Eq. (6), the coefficient ψ is the surface available for heterogeneous nucleation per unit bulk volume of liquid phase and ω is the geometric correction factor for the minimum work required to form a critical nucleus. For heterogeneous nucleation on a smooth surface with no cavities, these coefficients are given by

$$\psi = \frac{1}{2}(1 + \cos\theta) \tag{7}$$

$$\omega = \frac{1}{4}(1 + \cos\theta)^2(2 - \cos\theta) \tag{8}$$

It follows from Eqs. (5), (6), and (3) that

$$T_{nl} - T_s = \frac{T_s}{h_{fg}\rho_v}\sqrt{\frac{16\pi\sigma^3\omega}{3kT_{nl}\ln(N_0^{\gamma}kT_{nl}\psi/J\cdot h)}} \tag{9}$$

The above equation is applicable for both homogeneous nucleation (with $\gamma = \psi = \omega = 1$) and heterogeneous nucleation (with $\gamma = 2/3$ and ψ and ω given by Eqs. (7) and (8) respectively). Note also that the nucleation temperature T_{nl} determined from Eq. (9) is not sensitive with the chosen value of J. As commonly adopted in classical work [14,16], we can choose the value of $J_{hom} = 1\ cm^{-3}\ s^{-1}$ and $J_{het} = 1\ cm^{-2}\ s^{-1}$ for computation of T_{nl}. After the value of T_{nl} is determined, the curvature of the critical bubble nucleus r_c for homogeneous nucleation and heterogeneous nucleation on a surface can be determined from

$$r_c = \frac{2\sigma}{P_b - P_l} = \frac{2\sigma}{P_s(T_{nl}) - P_l} \tag{10}$$

Referring to Fig. 1, the value of y_b for homogeneous nucleation is

$$y_b = 2r_c \tag{11}$$

while for heterogeneous nucleation on a smooth surface is

$$y_b = r_c(1 + \cos\theta) \tag{12}$$

Table 1
Properties of water (at 1.013×10^5 Pa)

T_s (K)	σ (N m^{-1})	λ (W m^{-1} K^{-1})	ρ_l (kg m^{-3})	C_P (kJ kg^{-1} K^{-1})
373.15	0.05886	0.683	958.4	4.22

Table 2
The superheat limit and the critical parameters of water

J (cm^{-3} s^{-1})	T_{nl} (K)	r_c (nm)	P_v (MPa)	P_e (MPa)
1	576.8	3.15	8.72	9.08

Using the properties of water listed in Table 1, we can compute the homogeneous nucleation temperature from Eq. (9) and the critical nucleus radius from Eq. (10) to give $T_{nl} = 303.7\ ^\circ\text{C} = 576.8$ K and $r_c = 3.5$ nm, which are listed in Table 2.

As mentioned previously, the surface of the silicon microchannels fabricated by microfabrication technology is usually very smooth with sub-micron cavities. Thus, it can be speculated that the nucleation temperature of the liquid in a silicon microchannel will approach to the homogeneous nucleation temperature (or the superheat limit in liquid). Peng et al. [6] have reported a very high wall temperature, approximately 30 °C lower than the superheat limit calculated from Kwak's theory [7] for methanol during boiling in their triangular microchannel. However, the nucleation temperatures of water in other boiling heat transfer experiments in microchannels [8–11,20] were considerably lower than the homogeneous nucleation temperature of 303.7 °C as commonly accepted for water [16,18,19]. In fact, Jiang et al. [9] observed bubble generation at a subcooled temperature of 80 °C. This may be owing to the following reasons:

(i) *Heterogeneous nucleation on a surface with a large contact angle*

The effect of contact angle on nucleation temperatures T_{nl} for heterogeneous nucleation in water calculated from Eqs. (6)–(9), are presented in Fig. 3 where it is shown that the nucleation temperature decreases as the contact angle is increased. Although the contact angle θ may vary from 0° to 180°, the maximum contact angle measured from experiments is less than 140° [14]. For this reason, we only compute the values of T_{nl} and r_c for $\theta = 0^\circ$ to 140° in this article.

(ii) *Effect of corners in a microchannel*

In the previous work [9–11], it was observed that nucleation sites existed at channel corners. It should be noted that corners of a microchannel can be considered as pseudo microcavities due to their microscale size, which will decrease the nucleation temperature for the heterogeneous nucleation. Referred to Fig. 2, the geometric correction factor ω for minimum work required to form a critical nucleus at a corner (with an angle of 2β) of a smooth microchannel is,

$$\omega = \frac{\beta}{2\pi}(1+\cos\theta)^2(2-\cos\theta) \tag{13}$$

which is obtained from Eq. (8) by the multiplication of a geometric correction factor $2\beta/\pi$, representing the decrease in the bubble volume. Note that for microchannels with triangle, rectangle and trapezoidal cross-sectional areas, $2\beta \approx 60^\circ$, 90°, 120° respectively.

(iii) *Effect of dissolved-gases*

It should be noted that in the experiments conducted for boiling in microchannels [8–11,20], water in the reservoirs was usually driven by a compressed gas [9–11] or a pump [8,20], which was not degassed before the experiment. Indeed, Jiang et al. [9] indicated that dissolved gas existed in the liquid of their experiments, which caused subcooled boiling. In this connection, the effect of dissolved gas on boiling incipience and CHF has been investigated experimentally by You et al. [21]. Their results show that the dissolved gas lowers the nucleation temperature greatly when the dissolved gas content becomes high. Massoudi and King [22] studied the effect of different gas contents under different pressures on the surface tension of water–gas interface, and showed that the surface tension of water–N_2 had little variation. Forest and Ward [23] as well as Ward et al. [17] have analyzed the effect of dissolved gas on the homogeneous nucleation and heterogeneous nucleation in liquids respectively. According to Ward and his collaborators [17,23], the pressure in the vapor bubble is given by

$$P_b = P_{vb} + P_{gb} \tag{14}$$

where P_{vb} and P_{gb} are the partial pressure of vapor phase and gas phase respectively. If the isothermal compressibility of liquid is neglected, Ward et al. [17] gave

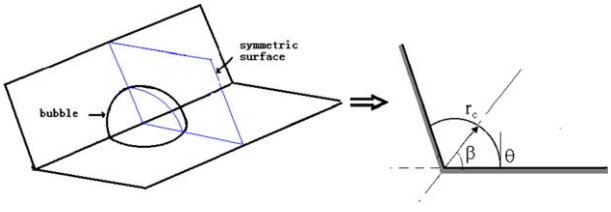

Fig. 2. Bubble cavitation model at the corner of the microchannel.

$$P_{vb} = P_s(T_{nl})\exp(-C_g) \tag{15}$$

$$P_{gb} = K_h C_g \tag{16}$$

where C_g is the solubility of the dissolved gas and K_h is the Henry constant.

Substituting Eqs. (14)–(16) into Eq. (6), a new expression for the nucleation temperature with the effect of dissolved gas taken into consideration is obtained as,

$$T_{nl} - T_s = \frac{T_s \exp(C_g)}{h_{fg}\rho_v}\left(\sqrt{\frac{16\pi\sigma^3\omega}{3kT_{nl}\ln(N_0^{\gamma}kT_{nl}\psi/J\cdot h)}} - K_h C_g\right) \tag{17}$$

Fig. 3 shows the effects of the contact angle θ (in the range from 50° to 110°), the dissolved air and the corner on the nucleation temperature of water. Curve 1 in Fig. 3 is calculated from Eq. (9) for water. Curve 2 is obtained from Eq. (17) with the saturated dissolved air in water and with the estimation of the 2% reduction in surface tension. The solubility of air in water at 100 °C and 1 atm is 11.5×10^{-3} ml/ml and K_h is 155×10^6 Pa l/mol [25] and these values were used in the computation. It can be seen from this figure that the nucleate temperature of water decreases from 270 to 240 °C as the contact angle is increased from 50° to 110° and the nucleation temperature will continue to decrease with further increase of the contact angle. In practice, it is rather difficult to determine or choose a proper value of the contact angle [24]. A comparison of curves 1 and 2 shows that the dissolved air can significantly decrease (about 35 °C) the bubble nucleation temperature. The three circles in Fig. 3 are the calculated cavitation temperatures of water in triangle, rectangle and trapezoidal microchannels (where $2\beta \approx 60°$, 90°, 120° respectively) at a specific contact angle of 90° (as an example), taking into consideration of the corner effect as well as dissolved air. It is shown that the cavitation temperature in a microchannel with triangular cross-section is the lowest (about 199 °C) among three kinds of channels. According to Eq. (10), the initial radius of the bubble nuclei of water increases from 3.15 to 18 nm when the nucleation temperature decreases from 303.7 to 199 °C.

(iv) *Residual vapor (gas)-trapped microcavities from the fabrication process*

The emergence of vapor (gas) from trapped microcavities due to elevated temperatures is the domain mechanism for bubble cavitation in comparatively large macrosystems. The cavitation temperature for this case can be obtained directly from the Hsu's theory and Eq. (4a) if the value of contact angle is given. The calculated results of temperature for bubble emergence given by Eq. (4a) with $\theta = 90°$ (consequently $r_m = r_c$ from Eq. (4)) are shown as curve 1 in Fig. 4. With the effect of dissolved gas taken into consideration, the cavitation temperature can be obtained directly from Eqs. (10) and (14)–(16) with the aid of Eq. (3) to give:

$$T_{nl} - T_s = \frac{T_s \exp(C_g)}{h_{fg}\rho_v}\left(\frac{2\sigma}{r} - K_h C_g\right) \tag{18}$$

Eq. (18), which is applicable for contact angle $\beta \leqslant \theta \leqslant \pi/2$ is presented as curve 2 in Fig. 4. It is shown that the effect of dissolved air will further decrease the bubble emergence temperature. Thus the temperature for trapped bubble (with radius greater than 1 μm) to emerge can be lower than the saturation temperature of 100 °C (subcooled boiling) because of the presence of the dissolved air, which is much lower than the nucleation

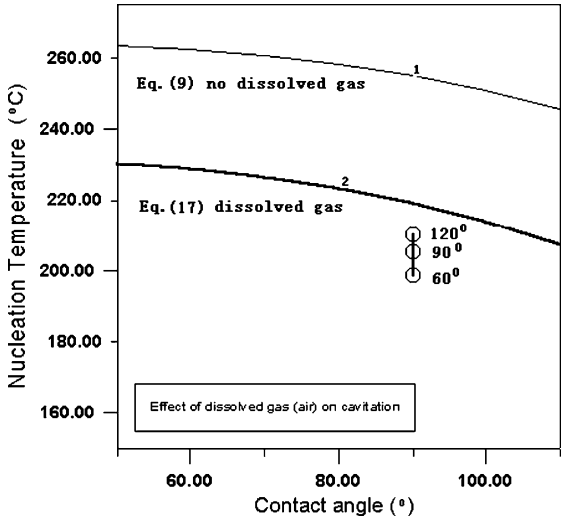

Fig. 3. Effects of dissolved air, corners, and contact angle on nucleation temperature of water.

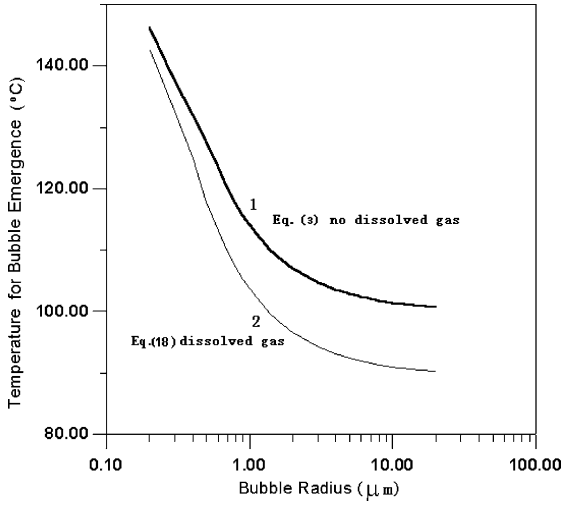

Fig. 4. Temperature necessary for comparatively large air bubble emergence in a microchannel.

temperature of water on smooth surface (above 200 °C as shown in Fig. 3).

From the above discussion, we can conclude that the nucleation temperature of a fluid may be considerably decreased because of the following effects: a comparatively large contact angle, dissolved gas in liquid, existence of corners in the microchannel, and randomly residual vapor (gas) trapped in microcavities. For these reasons, incipient boiling temperatures of water in existing microchannel experiments [8–11,20] are much lower than the superheat limit of 303.7 °C.

4. Effects of flow motion on bubble nucleation

In this section, we will consider effects of flow motion on bubble nucleation in microchannels in a MEMS device. For this purpose, consider a steady flow in a microchannel heated from below before the incipient boiling takes place. Note that microchannels in MEMS devices differ from macrochannels in conventional applications in two aspects: (1) instead of circular cross-section, microfabricated microchannels on silicon wafers, have trapezoidal or triangular cross-sectional areas if they are fabricated by anisotropic wet etching. The microchannels have rectangular cross-sectional areas if they are fabricated by DRIE or precise machining; and (2) instead of heated symmetrically as in macrochannels, the heat source is often added on one side of the microchannel.

4.1. Convective heat transfer in flowing liquids

We now consider a steady flow in a microchannel, with constant heat flux from below and constant wall temperature from the top, as shown in Fig. 5a. To simplify the problem, we consider only the 2D flow as shown in Fig. 5b. If a hydrodynamically fully-developed flow is assumed, the velocity profile of a single phase flow before incipient boiling taking place is given by

$$u(y) = 6u_{\mathrm{m}}\left[\frac{y}{\delta_{\mathrm{h}}} - \left(\frac{y}{\delta_{\mathrm{h}}}\right)^2\right] \tag{19}$$

where $u_{\mathrm{m}} = \dot{m}/\rho_{\mathrm{l}}A = \Delta P\delta_{\mathrm{h}}^2/12\mu_{\mathrm{l}}L$ is the mean flow velocity in the channel, $\dot{m}$ is the mass flow rate and A is the area of cross-section of the microchannels $A = \delta_{\mathrm{h}} \cdot \delta_{\mathrm{w}}$ (see Fig. 5a).

The energy equation for a hydrodynamically fully-developed flow is

$$u\frac{\partial T_{\mathrm{l}}}{\partial x} = \frac{\lambda_{\mathrm{l}}}{C_P\rho_{\mathrm{l}}}\frac{\partial^2 T_{\mathrm{l}}}{\partial y^2} \tag{20}$$

where u is given by Eq. (19). Eq. (20) is to be solved subject to the following boundary conditions

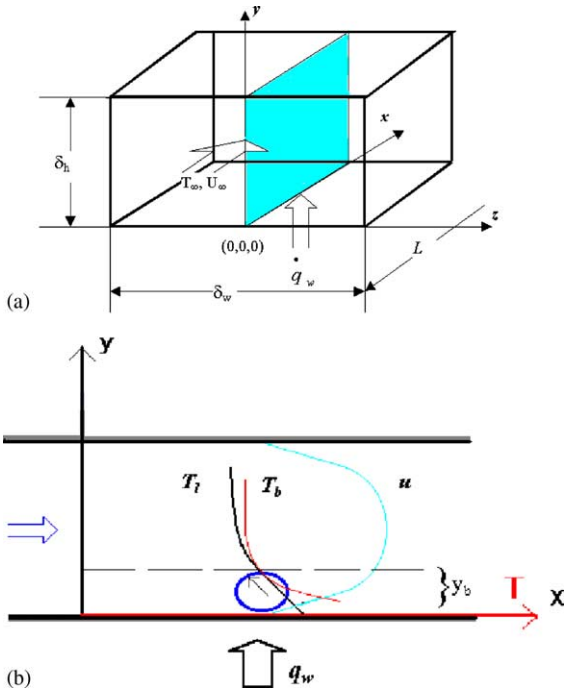

Fig. 5. Incipient flow boiling in a microchannel: (a) 3-D model, (b) 2-D simplified model.

$$y = 0, \quad -\lambda_{\mathrm{l}}\left.\frac{\partial T_{\mathrm{l}}}{\partial y}\right|_{y=0} = \dot{q}_{\mathrm{w}} \tag{21a}$$

$$y = \delta_{\mathrm{h}}, \quad T_{\mathrm{l}} = T_{\mathrm{w}} \tag{21b}$$

$$x = 0, \quad T_{\mathrm{l}} = T_i \tag{21c}$$

$$x = L, \quad -\lambda_{\mathrm{l}}\left.\frac{\partial T_{\mathrm{l}}}{\partial y}\right|_{x=L} = 0 \tag{21d}$$

Since it is not possible to obtain an analytical solution to Eqs. (20)–(21), a numerical solution with tri-diagonal matrix algorithm (TDMA) was used to obtain the temperature distribution $T_{\mathrm{l}}(x, y)$.

4.2. Incipient boiling in a microchannel

In order to study how a bubble in flowing water will survive in a microchannel based on the present model, a simulation was carried out for flow in a microchannel with $\delta_{\mathrm{h}} = 60$ μm, $\delta_{\mathrm{w}} = 60$ μm, $L = 1$ cm and with $T_{\mathrm{w}} = T_i = T_\infty = 25$ °C. If Hsu's concept for bubble survival is adopted, nucleation will be initiated when

$$T_{\mathrm{l}}(x, y_{\mathrm{b}}) \geqslant T_{\mathrm{nl}} \tag{22}$$

which corresponds to Eq. (1) where T_{b} is replaced by T_{nl} that was computed in Section 3. Note that the numerical results are no longer valid in the region when $T_{\mathrm{l}}(x, y) \geqslant T_{\mathrm{nl}}$ since the governing equations given by Eqs. (19)–(20) are applicable only for a single-phase flow.

To show the effects of mass flow rate and heat flux on bubble nucleation in a microchannel, numerical solutions of Eqs. (20)–(21) were carried out for the following two cases:

Case 1: the effect of mass flow rate on incipient boiling in a microchannel at a constant heat flux $q_w = 300$ W/cm^2 is studied. The numerical results for velocity profiles and temperature profiles at mass flow rates of 0, 0.06, 0.6, 6 mg/s are presented in Fig. 6 and Figs. 7–10 respectively. Fig. 6 shows that the velocity profiles in the microchannel at the four different mass flow rates are of parabolic shapes. These velocity profiles were computed based on Eq. (19) that are independent of heat flux. Figs. 7–10 show the vertical temperature profiles at different x locations (100, 1000, 10,000 μm)

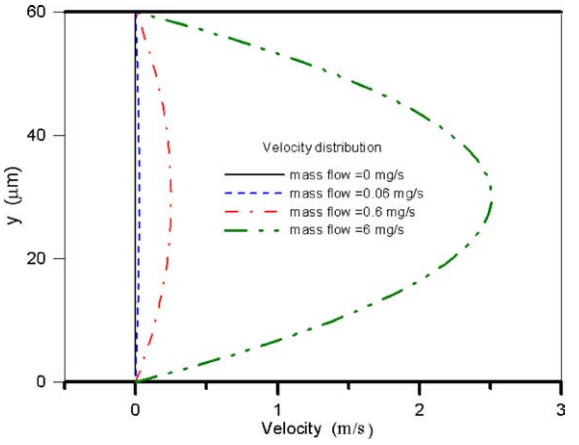

Fig. 6. Effects of mass flow rates on velocity profiles.

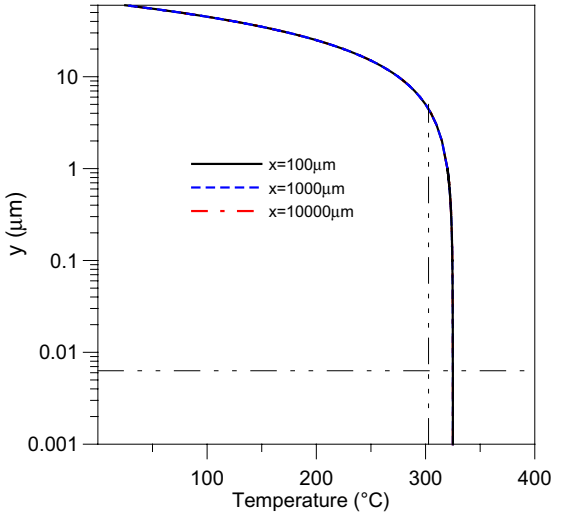

Fig. 7. Temperature profiles at different locations at zero mass flow rate and $q_w = 300$ W/cm^2.

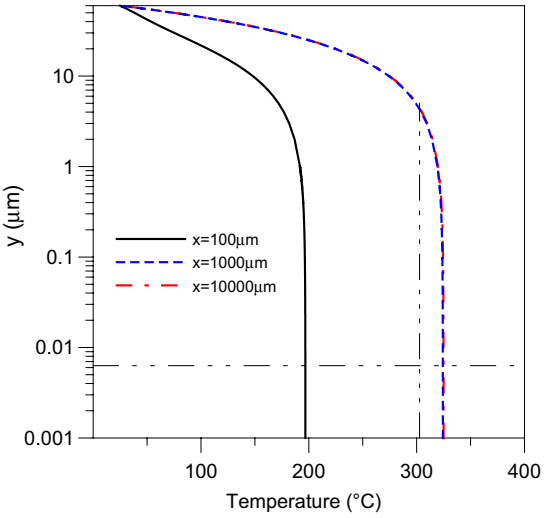

Fig. 8. Temperature profiles at different x locations at a mass flow rate $\dot{m} = 0.06$ mg/s and $q_w = 300$ W/cm^2.

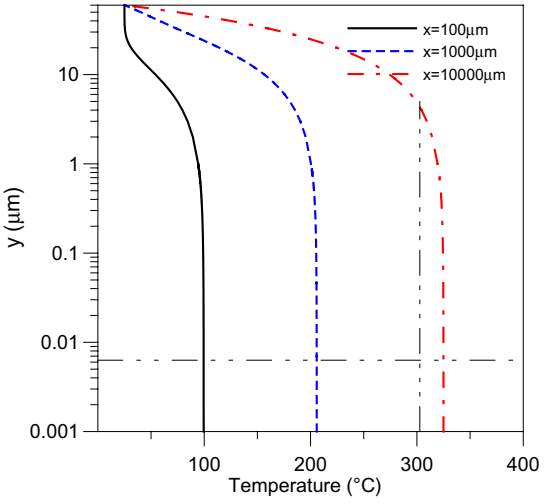

Fig. 9. Temperature profiles at different x locations at a mass flow rate $\dot{m} = 0.6$ mg/s and $q_w = 300$ W/cm^2.

for four mass flow rates respectively. In these figures, the horizontal and vertical dot-dashed lines represent the projection height of vapor bubble $y_b = 6.3$ nm, and the nucleation temperature of 303.7 °C based on the homogeneous nucleation model of pure water. The horizontal dashed lines are plotted to indicate the bubble size relative to the height of the microchannel. The vertical dashed lines are plotted to identify the nucleation location based on the criterion given by Eq. (22), and as discussed earlier, the numerical results are no longer valid in the region $T_l(x, y) \geqslant T_{nl}$ i.e., after the incipient boiling takes place. If the nucleation temperature is lower than those given by the homogeneous

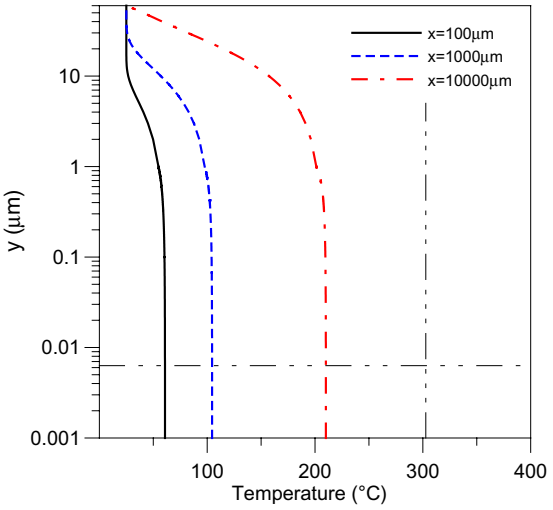

Fig. 10. Temperature profiles at different x locations at a mass flow rate $\dot{m} = 6$ mg/s and $q_w = 300$ W/cm^2.

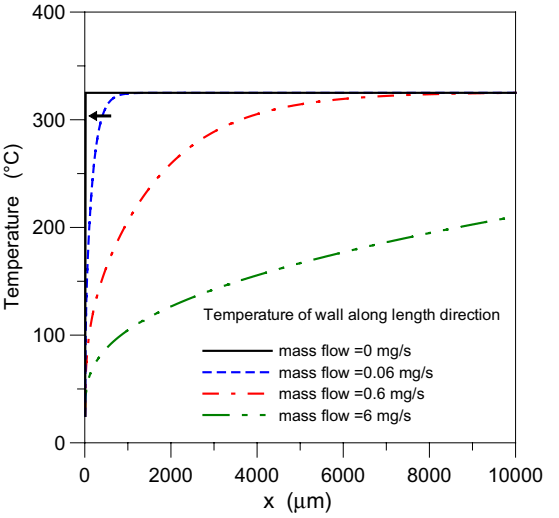

Fig. 11. Effects of mass flow rate on surface temperatures along the x-direction at $q_w = 300$ W/cm^2.

nucleation model because of dissolved gas and the existence of cavities or corners, the vertical dashed lines will move to the left. Similarly, the horizontal dashed lines may be higher because of these effects. Note that temperature distributions in Figs. 7–10 are plotted in a semilog scale so that the temperature profile near the wall at $y = 0$ can be clearly shown. For this reason, the vertical temperature profiles in these figures are distorted. Fig. 7 shows the temperature profiles are independent of x if no mass flow. A comparison of Figs. 7–10 shows that higher mass flow rate will cause lower temperature in the microchannel as expected. Furthermore, it can be seen that if the height of microchannel is large compared to y_b, the temperature gradient is quite small when $y < 0.1$ μm, no matter what the mass flow rate is. Thus, if the height of microchannel is large enough and the wall temperature is higher than the nucleation temperature T_{nl} or T_b, the condition $T_l(x, y_b) \geqslant T_b$ will be satisfied automatically. Therefore, in a relatively large microchannel or in a macrochannel, we can simply consider the wall temperature in order to determine whether boiling would occur. However, it should be noted that the present model is not applicable when the height of the microchannel is comparable to the size of bubble, i.e., a nanochannel. Under this situation, molecular dynamics simulation is needed to examine the mechanism of bubble nucleation in such a nanochannel [26].

The effects of mass flow rates on surface temperatures along the x-direction at $q_w = 300$ W/cm^2 are shown in Fig. 11. The arrow points to the homogeneous nucleation temperature of 303.7 °C. It is seen from Fig. 11 that for a microchannel with length $L = 1$ cm at constant heat flux $q_w = 300$ W/cm^2, there exist different heat transfer modes: at a low mass flow rate ($\dot{m} = 0.06$ mg/s for example) most part of the channel will nucleate; on the other hand at a higher mass flow rate ($\dot{m} = 6$ mg/s for example) there will be no bubble nucleation in the microchannel.

Case 2: the effects of heat flux on incipient boiling at a constant mass flow rate $\dot{m} = 0.6$ mg/s (i.e., $u_m = 0.167$ m/s) are studied. Computations were carried out for heat fluxes of $q_w = 250, 300, 350$ W/cm^2 at the same mass flux of $\dot{m} = 0.6$ mg/s. The numerical results are presented in Fig. 12 where it can be seen that no bubble nucleation in

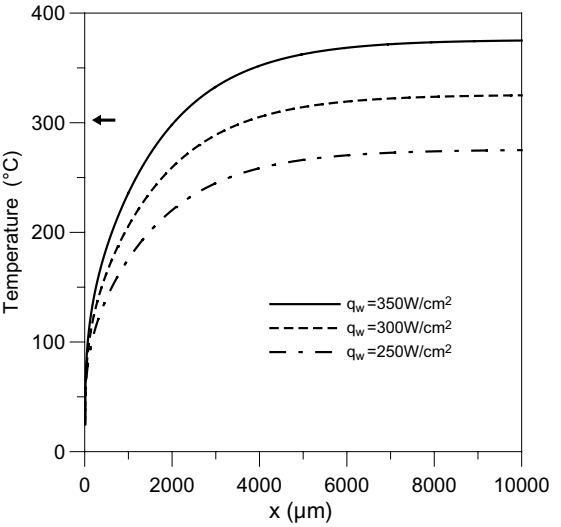

Fig. 12. Effects of heat flux on surface temperature along x-direction at a mass flow rate $\dot{m} = 0.6$ mg/s.

the microchannel at low heat fluxes; on the other hand, nucleate boiling occurs in most part of the microchannel at higher heat fluxes.

From the above discussions, we can conclude that the governing parameters on bubble nucleation in microchannels are: hydraulic diameter and length of the microchannel, mass flow rate, heat flux on the heater surface, nucleation temperature in liquids as determined from Section 3, inlet temperature of the fluid, and top wall temperature of the microchannel.

4.3. Suppression of forming visible bubbles by flow motion

Mitrovic [27] argued that after bubble nucleation, the bubbles adhere to the microchannel wall will be swept away because of the large shear stress and the lift force. As a result, the bubble size at detachment is smaller at a smaller channel for a given mass flow rate. This effect leads to a stronger suppression of visible bubbles formation in flow boiling in a microchannel. Thus, Mitroic's argument together with the present model, shows that bubble nucleation may be suppressed by a sufficiently high velocity, which may be the reason why some investigators were unable to observe bubble generation in microchannels [6].

5. Concluding remarks

The following conclusions can be drawn from this work:

(1) A large contact angle between the fluid and the substrate, and the existence of dissolved gas, randomly residual vapor (gas)-trapped, and corners can effectively lower the nucleation temperature in a microchannel. These effects may be responsible for the experimental observation that the nucleation temperature in a microchannel is lower than those computed based on classical theory of homogeneous nucleation temperature in spite of the fact that the silicon microchannel is smooth.

(2) The effects of microchannel size, mass flow rate and heat flux on boiling incipience or bubble cavitation in a microchannel are studied based on an extension of Hsu's concept on the survival of a bubble cavity in pool boiling and with the aid of kinetics of nucleation and a convective heat transfer analysis. In particular, the effects of mass flow rate on incipient heat flux and temperature distribution during incipient boiling in the microchannel are presented. It is shown that a large flow rate may suppress bubble generation in a microchannel. It should be noted that the numerical model presented in this paper is a primitive one since heat conduction in the substrate has been neglected. Because of the high thermal conductivity of the silicon substrate, axial heat conduction in the substrate may play an important role in the heat transfer process. A three-dimensional conjugate heat transfer simulation should be carried out in order to compare with experimental results.

Acknowledgements

This work was supported by the Research Grant Council of Hong Kong SAR through the research grant HKUST6014/02E. The authors would like to thank the reviewers for their valuable comments. They would also like to thank Dr. H.Y. Wu, Ms. J.T. Cui, Mr. G.N. Liu and Mr. Chin Pang Billy Siu for their help during the course of this study.

References

[1] I. Mudawar, Assessment of high-heat-flux thermal management schemes, IEEE T Compon Pack T 24 (2) (2001) 122–141.
[2] L. Lin, Microscale thermal bubble formation: thermophysical phenomena and applications, Microscale Thermophys. Eng. 2 (1998) 71–85.
[3] A. Asai, Bubble dynamics in boiling under high heat flux pulse heating, ASME J. Heat Transfer 113 (1991) 973.
[4] Y. Hao, H.N. Oguz, A. Prosperetti, The action of pressure–radiation forces on pulsating vapor bubbles, Phys. Fluids 13 (5) (2001) 1167–1177.
[5] K. Takahashi, et al., Novel applications of thermally controlled microbubble driving system, in: The 14th IEEE International Conference on MEMS, 2001, pp. 286–289.
[6] J.T. Zhang, X.F. Peng, G.P. Peterson, Analysis of phase-change mechanisms in microchannels using cluster nucleation theory, Microscale Thermophys. Eng. 4 (2000) 177–187.
[7] H.Y. Kwak, Y.W. Kim, Homogeneous nucleation and macroscopic growth of gas bubble in organic solutions, Int. J. Heat Mass Transfer 41 (4–5) (1998) 757–767.
[8] L. Jiang, M. Wong, Y. Zohar, Forced convection boiling in a microchannel heat sink, J. Microelectromech. Sys. 10 (1) (2001) 80–87.
[9] W. Qu, I. Mudawar, Prediction and measurement of incipient boiling heat flux in micro-channel heat sink, Int. J. Heat Mass Transfer 45 (2002) 3933–3945.
[10] H.Y. Wu, P. Cheng, Boiling instability in parallel silicon microchannels at different heat flux, Int. J. Heat Mass Transfer 46 (2003) 2603–2614.
[11] H.Y. Wu, P. Cheng, Three boiling instability modes in microchannels, presented at ASME Summer Heat Transfer Conference, Las Vegas, USA, July 20–24, 2003.
[12] Y.Y. Hsu, On the size range of active nucleation cavities on a heating surface, ASME J. Heat Transfer 84 (1962) 207–216.
[13] Y.-Y. Hsu, R.W. Graham, Transport Processes in Boiling and Two-Phase Systems, Hemisphere, Washington, DC, 1976.
[14] R. Cole, Boiling Nucleation, in: Advances in Heat Transfer, vol. 10, Academic Press, Inc., 1974, pp. 86–166.

[15] S.G. Bankoff, T. Haute, Ebullition from solid surfaces in the absence of a pre-existing gaseous phase, Trans. ASME (1957) 735–740.
[16] M. Blander, J.L. Katz, Bubble nucleation in liquids, AIChE J. 21 (5) (1975) 833–848.
[17] C.A. Ward, W.R. Johnson, R.D. Ventor, S. Ho, T.W. Forest, W.D. Fraser, Heterogeneous bubble nucleation and conditions for growth in a liquid–gas system of constant mass and volume, J. Appl. Phys. 54 (4) (1983) 1833–1843.
[18] V.P. Skripov, Metastable Liquids, John Wiley & Sons, New York, 1974.
[19] C.T. Avedisian, The homogeneous nucleation limits of liquids, J. Phys. Chem. Ref. Data 14 (3) (1985) 695–729.
[20] L. Zhang, J.-M. Koo, L. Jiang, M. Asheghi, K.E. Goodson, J.G. Santiago, T.W. Kenny, Measurements and modeling of two-phase flow in microchannels with nearly constant heat flux boundary conditions, J. Microelectromech. Syst. 11 (1) (2002) 12–19.
[21] S.M. You, T.W. Simon, A. Bar-Cohen, Y.S. Hong, Effects of dissolved gas content on pool boiling of a highly wetting fluid, ASME J. Heat Transfer 117 (1995) 687–692.
[22] R. Massoudi, A.D. King Jr., Effect of pressure on the surface tension of water. Adsorption of low molecular weight gases on water at 25 °C, J. Phys. Chem. 76 (22) (1974) 2262–2268.
[23] T.W. Forest, C.A. Ward, Homogeneous nucleation of bubbles in solutions of pressures above the vapor pressure of pure liquid, J. Chem. Phys. 69 (5) (1978) 2221–2230.
[24] F.G. Tseng, C.Y. Huang, C.C. Chieng, H. Huang, C.S. Liu, Size effect on surface tension and contact angle between protein solution and silicon compound, PC, and PUMMA substrate, Microscale Thermophys. Eng. 6 (2002) 31–53.
[25] Handbook of Chemistry and Physics, 55th edition, CRC Press, Cleveland, OH, 1974.
[26] G. Nagayama, T. Tsuruta, P. Cheng, Molecular dynamics simulation on bubble formation of microscale fluidic flow. Proc. of the 1st International Symposium on Micro & Nano Technology (ISMNT-1), Honolulu, Hawaii, March 14–17, 2004.
[27] J. Mitrovic, Survival conditions of a vapour bubble in saturated liquid flowing inside a micro-channel, Int. J. Heat Mass Transfer 44 (11) (2001) 2177–2181.